Sound propagation in rigid bends: A multimodal approach

S. Félix, and V. Pagneux

Citation: The Journal of the Acoustical Society of America **110**, 1329 (2001); doi: 10.1121/1.1391249
View online: https://doi.org/10.1121/1.1391249
View Table of Contents: https://asa.scitation.org/toc/jas/110/3
Published by the Acoustical Society of America

Sound propagation in rigid bends: A multimodal approach

S. Félix[a] and V. Pagneux
Laboratoire d'Acoustique de l'Université du Maine, UMR-CNRS 6613, Université du Maine, Avenue Olivier Messiaen, 72085 Le Mans Cedex 09, France

(Received 1 February 2001; revised 11 June 2001; accepted 13 June 2001)

The sound propagation in a waveguide with bend of finite constant curvature is analyzed using multimodal decomposition. Two infinite first-order differential equations are constructed for the pressure and velocity in the bend, projected on the local transverse modes. A Riccati equation for the impedance matrix is then derived, which can be numerically integrated after truncation at a sufficient number of modes. An example of validation is considered and results show the accuracy of the method and its suitability for the formulation of radiation conditions. Reflection and transmission coefficients are also computed, showing the importance of higher order mode generation at the junction between the bend and the straight ducts. The case of varying cross-section curved ducts is also considered using multimodal decomposition. © *2001 Acoustical Society of America.* [DOI: 10.1121/1.1391249]

PACS numbers: 43.20.Mv [ANN]

I. INTRODUCTION

Because the study of the propagation in curved ducts appears as a logical extension to the theory of the propagation of acoustics and electromagnetic fields in straight waveguides, it has aroused a number of works and papers (for a review in acoustics, see Rostafinski[1]).

The most classical way of solving the problem is the method of separation of variables,[2–6] leading to the calculation of modes in the bend. In the sequel we will call this approach the ''bend mode method'' (BMM). Indeed, for a circular bend of rectangular cross section, and in particular for a two-dimensional circular bend, the equations of motion are known to be separable. However, for a bend of finite length this solution must be joined to the wave solutions of the adjoining straight ducts. To avoid the problem, Krasnushkin,[2] Grigor'yan,[3] and others restricted themselves to consideration of infinitely long bends. The case of a bend joining two straight ducts was treated by Rostafinski,[4] Cummings,[5] and Osborne,[6] by using the BMM.

The dispersion relation for bend modes involves Bessel functions of noninteger order. In view of these difficulties due to the implicit dispersion relation, approximations were proposed. Krasnushkin[2] adopted a perturbation method and treated only the case of slightly bent tubes. Grigor'yan[3] developed a method of power-series expansion of the expressions involving the Bessel functions. Rostafinski[4] restricted his investigation to very low frequencies, and also expanded the Bessel functions in terms of increasing powers of their argument. Cummings[5] considered only the propagation of the plane wave mode, and Osborne[6] used a simplified theory, notably in considering only the propagating modes.

Methods different from the BMM have been used, such as the Galerkin method (Tam[7]), finite differences method (Cabelli[8]) or more recently a method based on parabolic approximation (Dougherty[9]). Such approaches permit to investigate more general cases than those, restricted, presented previously, and are powerful to yield information. Nevertheless, generally, they do not allow a direct physical interpretation, and are not always convenient for formulating radiation conditions.

In this context we propose to formulate a multimodal method (MMM) to determine the wave propagation in two-dimensional rigid circular bends of any dimension and at any frequency. Such study for ducts of straight longitudinal axis was done by Pagneux *et al.*,[10,11] who proposed and used successfully a multimodal method for calculating the wave propagation in varying cross-section waveguides. Following works done by Stevenson,[12] Albertson,[13] Roure,[14] and Kergomard,[15] they constructed two infinite first-order differential equations for the components of the pressure and of the axial velocity projected onto the normal modes. Then they derived a new equation for the impedance matrix which is numerically workable. Tam[7] adopted a quite similar approach, using the local transverse modes to construct a set of basis functions for calculating the solution of the Euler equations in a circular bend of constant cross section by the Galerkin method. He gave a very interesting algebraic calculation of the reflection and transmission matrices. Results were, on the other hand, limited to tables of values, without particular applications. A similar algebraic approach is presented in the appendix.

In Sec. II of this paper, the modal method described previously is formulated for circular bends of constant cross section, pointing out the suitability of this approach for the formulation of radiation conditions, and the possibility to access rapidly to the impedance, and consequently to the input impedance and reflection coefficient. A particular example is treated in Sec. III, for which an analytical solution can be found, allowing the proposed method to be validated. Section IV presents several applications, showing the accuracy and advantages of the present method. Finally, in Sec. V, the multimodal approach is extended to varying cross-section curved ducts, and results are presented.

II. EQUATIONS AND BOUNDARY CONDITIONS

The general duct system to be analyzed here is shown in Fig. 1; it consists of a two-dimensional circular bend which

[a]Electronic mail: simon.felix@univ-lemans.fr

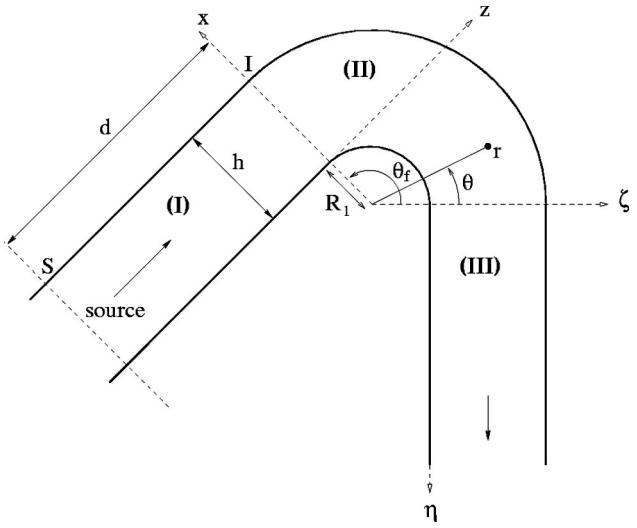

FIG. 1. Geometry of the duct system with bend and systems of coordinates.

joins rigid straight ducts. The parameters of the bend are its overall angle θ_f, inner radius R_1 and width h. A source generates sound upstream from the bend, and a radiation condition is imposed at the outlet.

A. Formulation

Throughout this paper adiabatic lossless linear media will be assumed. The acoustic velocity $\hat{\mathbf{v}}$ and the acoustic pressure $\hat{p}$ satisfy the equation of mass conservation

$$\boldsymbol{\nabla}\cdot\hat{\mathbf{v}} = -\frac{j\omega}{\rho_0 c_0^2}\hat{p}, \tag{1}$$

and the equation of momentum conservation

$$j\omega\hat{\mathbf{v}} = -\frac{1}{\rho_0}\boldsymbol{\nabla}\hat{p}, \tag{2}$$

the caret " ˆ " denoting dimensional quantities and time dependence $\exp(j\omega t)$ being omitted. $\hat{\mathbf{v}}$ has components $(\hat{v}_r, \hat{v}_\theta)$, ρ_0 is the density of air, and c_0 is the speed of sound.

The reference pressure $\rho_0 c_0^2$ and velocity c_0 are used to reduce Eqs. (1) and (2) to dimensionless terms, and we introduce the frequency $k=\omega/c_0$, so that these equations become

$$\boldsymbol{\nabla}\cdot\mathbf{v} = -jkp, \tag{3}$$

$$-jk\mathbf{v} = \boldsymbol{\nabla}p. \tag{4}$$

By eliminating v_r these equations give in the bend

$$-jkrp = \frac{\partial v_\theta}{\partial\theta} - \frac{1}{jk}\frac{\partial}{\partial r}\left(r\frac{\partial p}{\partial r}\right), \tag{5}$$

$$-jkrv_\theta = \frac{\partial p}{\partial\theta}. \tag{6}$$

Pressure p and axial velocity v_θ are now expressed using infinite series

$$p(r,\theta) = \sum_n \psi_n(r)P_n(\theta), \tag{7}$$

$$v_\theta(r,\theta) = \sum_n \psi_n(r)U_n(\theta), \tag{8}$$

where P_n and U_n are scalar coefficients, and ψ_n are the eigenfunctions obeying the transverse eigenproblem $\partial_{r^2}^2\psi_n = -\alpha_n^2\psi_n$, with the homogeneous Neumann boundary condition on the walls:

$$\left(\frac{\partial\psi_n}{\partial r}\right)_{r=R_1,R_1+h} = 0, \tag{9}$$

and the orthogonality relation

$$\int_{R_1}^{R_1+h}\psi_m(r)\psi_n(r)\,dr = \delta_{mn}. \tag{10}$$

These functions ψ_n are

$$\psi_n(r) = A_n\cos\left(\frac{n\pi}{h}(r-R_1)\right), \tag{11}$$

where

$$A_n = \sqrt{\frac{2-\delta_{n0}}{h}},$$

with the associated eigenvalues $\alpha_n = n\pi/h$. They are the classical transverse modes in a straight duct.

Following the matricial terminology, modal decompositions (7) and (8) will be written as

$$p = {}^t\boldsymbol{\psi}\mathbf{P}, \tag{12}$$

$$v_\theta = {}^t\boldsymbol{\psi}\mathbf{U}, \tag{13}$$

where $\mathbf{P}=(P_n)_{n\geqslant 0}$, $\mathbf{U}=(U_n)_{n\geqslant 0}$, and $\boldsymbol{\psi}=(\psi_n)_{n\geqslant 0}$ are columns vectors.

Then, by projecting Eqs. (5) and (6) on the functions ψ_n (see Appendix A), the following equations are obtained:

$$\mathbf{U}' = \frac{1}{jk}(C+KB)\mathbf{P}, \tag{14}$$

$$\mathbf{P}' = -jkB\mathbf{U}, \tag{15}$$

with matrices K, B, and C given by (see Appendix B)

$$K_{mn} = (k^2-\alpha_m^2)\,\delta_{mn}, \tag{16}$$

$$B_{mn} = \int_{R_1}^{R_1+h} r\psi_n(r)\psi_m(r)\,dr, \tag{17}$$

$$C_{mn} = \int_{R_1}^{R_1+h}\psi_n(r)\psi_m'(r)\,dr. \tag{18}$$

Because of the presence of evanescent modes (corresponding to $k^2-\alpha_m^2<0$), Eqs. (14) and (15) are numerically unstable,[10,11] and cannot be integrated directly. Therefore, following Ref. 10, an impedance matrix is defined, fulfilling

$$\mathbf{P} = Z\mathbf{U}. \tag{19}$$

Thus, by substituting $\mathbf{P}'$ and $\mathbf{U}'$ from Eqs. (14) and (15) in the derivation of Eq. (19), $\mathbf{P}'=Z'\mathbf{U}+Z\mathbf{U}'$, a Riccati equation for Z can be obtained:

$$Z'=-jkB-\frac{1}{jk}Z(C+KB)Z. \tag{20}$$

This first-order differential equation allows us to obtain the impedance matrix at the inlet, once the radiation condition (i.e., impedance matrix) is given at the outlet.

B. Boundary conditions

A radiation condition downstream from the bend is defined, which gives an initial condition for the Riccati equation (20). In the case of a bend terminated by a semi-infinite straight duct, as shown in Fig. 1, the radiation impedance is the characteristic impedance matrix, which is diagonal and given by

$$Z_{c_n}=-\frac{k}{k_n}, \tag{21}$$

where $k_n=\sqrt{k^2-\alpha_n^2}$ for propagative modes, $k_n=-j\sqrt{\alpha_n^2-k^2}$ for evanescent modes.

With this radiation condition Z can be calculated everywhere in the duct, since it is governed by a first-order differential equation [Eq. (20)]. To know the acoustic field, it is then possible to apply a boundary condition upstream, characterized as a known velocity or pressure, so once the impedance is found the pressure or velocity can be calculated as follows: we substitute Eq. (19) in Eq. (15) [respectively, (14)] to obtain

$$\mathbf{P}'=-jkBY\mathbf{P}, \tag{22}$$

respectively,

$$\mathbf{U}'=\frac{1}{jk}(C+KB)Z\mathbf{U}, \tag{23}$$

where Y is the admittance matrix ($Y=Z^{-1}$). Equation (22) [respectively, (23)] can be integrated from the inlet to the radiating end, giving $\mathbf{P}$ (respectively, $\mathbf{U}$). Afterwards the velocity (respectively, pressure) can be calculated, once $\mathbf{P}$ (respectively, $\mathbf{U}$) and Z are known. In contrast to direct numerical integration of Eq. (14) or Eq. (15), the integration of Eq. (22) or Eq. (23) is numerically stable because of the presence of the impedance matrix (see Ref. 10 for more details).

C. Numerical procedures

The numerical procedure adopted here is the same as used by Pagneux *et al.*[10] After truncation at a sufficient number of modes, the Riccati equation for Z is integrated down to the inlet of the bend using Runge–Kutta algorithms, with an adaptive step size. Z being stored on a grid of regularly spaced points along the axis, the integration of Eq. (23) in the opposite direction allows the calculation of the pressure and velocity fields.

Just as any radiation condition can be easily considered (except a tube closed by a rigid wall that necessitates putting attenuation in the model), the integration of Z, $\mathbf{U}$, and $\mathbf{P}$ can be extended to any type of waveguide upstream from the bend (see Appendix C). In contrast, when using the BMM, the formulation and computation of the continuity equations at the discontinuity between the bend and a joined duct may lead to mathematical and numerical difficulties (notably in term of convergence, see Ref. 16). More generally, joining solutions developed on different basis of functions may be a source of numerical difficulties. The iterative calculation of the impedance matrix along a system of joined ducts avoids such difficulties.

III. VALIDATION

To validate our method, we consider in this section a particular case of propagation in a bend for which an analytical solution can be found: the propagation of the first bend mode. The analytical and the multimodal approaches are compared and discussed.

As mentioned above, the Helmholtz equation is separable in the cylindrical coordinate system, and consequently there exists solutions of the type $p(r,\theta)=R(r)\Theta(\theta)$. These modes are characterized in the bend by a dimensionless wave number called (following Krasnushkin[2]) ''angular wave number.'' For a hard-wall bend these angular wave numbers may be real or pure imaginary numbers, corresponding, respectively, to propagative, and evanescent modes. We can thus sort them in decreasing order of their square values and call the first ν_0. In this paragraph, we are interested in calculating the first bend mode, characterized by ν_0, in order to validate our multimodal method with this solution.

A. Analytical solution

For any geometry of infinite bend, whatever its curvature, the Helmholtz equation for the acoustic pressure can be solved by separation of variables, to obtain the general solution

$$p(r,\theta)=\sum_{n\geqslant 0}(\alpha_n e^{j\nu_n\theta}+\beta_n e^{-j\nu_n\theta})[Y'_{\nu_n}(kR_1)J_{\nu_n}(kr) - J'_{\nu_n}(kR_1)Y_{\nu_n}(kr)], \tag{24}$$

obeying the homogeneous Neumann conditions ($\partial_r p=0$) on the walls ($r=R_1$ and R_1+h). Angular wave numbers ν_n are the solutions of the dispersion relation (see Krasnushkin[2])

$$J'_\nu(kR_1)Y'_\nu(k(R_1+h))-J'_\nu(k(R_1+h))Y'_\nu(kR_1)=0 \tag{25}$$

for a given value of $k=\omega/c_0$, and where J_ν and Y_ν are the Bessel functions of first and second kinds.

For a finite bend, expression (24) is also an exact analytical solution, but with boundary conditions at the inlet and the outlet that have to be determined. This point is studied in the following paragraph. In the sequel we will be interested in the first bend mode

$$p(r,\theta)=\alpha_0 e^{j\nu_0\theta}[Y'_{\nu_0}(kR_1)J_{\nu_0}(kr) - J'_{\nu_0}(kR_1)Y_{\nu_0}(kr)], \tag{26}$$

and we want to validate the multimodal approach with this known exact solution.

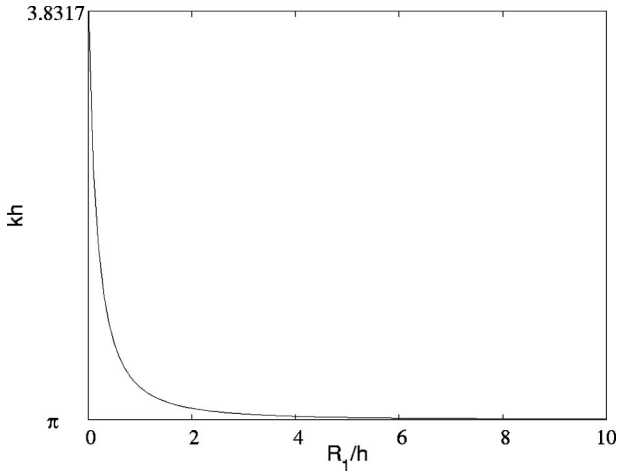

FIG. 2. First cutoff frequency in an infinite bend, as a function of the ratio R_1/h.

B. Multimodal approach

As mentioned previously (Sec. II B), we need an initial condition for the Riccati equation (20). We project the relation obtained from the exact solution (26)

$$\frac{\partial p}{\partial \theta} = j\nu_0 p \tag{27}$$

over the modes ψ_n to calculate the equivalent boundary condition for the impedance at the outlet ($\theta = 0$):

$$Z = -\frac{k}{\nu_0} B. \tag{28}$$

At the inlet of the bend, $\mathbf{P}(\theta_f)$ is given by projection of Eq. (26) over the ψ_n. This yields:

$$P_n(\theta_f) = A_n \alpha_0 e^{j\nu_0\theta_f} \int_{R_1}^{R_1+h} [Y'_{\nu_0}(kR_1) J_{\nu_0}(kr) - J'_{\nu_0}(kR_1) Y_{\nu_0}(kr)] \cos\left[\frac{n\pi}{h}(r-R_1)\right] dr. \tag{29}$$

C. Results

The source frequency is chosen under the first cutoff frequency in the bend; this cutoff frequency k is the first nonzero solution of

$$J'_0(kR_1) Y'_0(k(R_1+h)) - J'_0(k(R_1+h)) Y'_0(kR_1) = 0 \tag{30}$$

(see Osborne[6]). Figure 2 shows this cutoff frequency adimensioned with the duct width h, as a function of R_1/h. It is always larger than π—the first cutoff in a straight duct—and tends toward this value for extremely large ratio R_1/h, as expected. In our case, the geometry of the bend will be given by $R_1/h = 0.5$. This gives for the solution kh of Eq. (30) a value of 3.27. We then take an overall angle $\theta_f = \pi/2$ and a frequency such that $kh = \pi/4$, for which the angular wave number ν_0 equals 0.76.

Figure 3 shows the isopressure contours calculated using respectively the exact analytical expression (26) and the MMM, the pressure being in this case computed as described

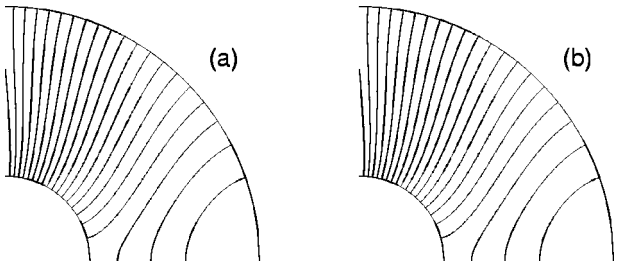

FIG. 3. Contour of the real part of pressure in a bend for the first angular mode, calculated (a) analytically, (b) using the MMM ($\theta_f = \pi/2$, $h/R_1 = 2$, $kh = \pi/4$).

in Sec. II C, with 17 modes. The results obtained by the modal decomposition agree perfectly with those calculated analytically [Eq. (26)]. As an example of check, the multimodal approach gives a pressure field with modulus independent of the axial coordinate θ and with a phase independent of r, as expected with expression (26). The maximum range compared to the mean value in both cases is less than 0.001%.

In order to measure the rate of convergence of the multimodal method, the analytical result (26) is chosen as the reference, and we define the error as follows:

$$\epsilon = \left(\frac{\int_0^{\theta_f}\int_{R_1}^{R_1+h} \|p - p_{\text{ref}}\|^2 r\, dr\, d\theta}{\int_0^{\theta_f}\int_{R_1}^{R_1+h} \|p_{\text{ref}}\|^2 r\, dr\, d\theta} \right)^{1/2}. \tag{31}$$

The error ϵ is shown in Fig. 4: it decreases monotically as more modes are introduced in the calculation. The convergence follows a $1/N^{3.23\pm0.1}$ law, N being the number of modes taken into account in the calculation. Thus the solution of the modal approach rapidly converges on the exact solution.

D. Conclusion of the validation

The multimodal method is validated, giving results in almost prefect agreement with the analytical solution in the example developed previously. Because this calculation is not limited to particular values of the geometrical and fre-

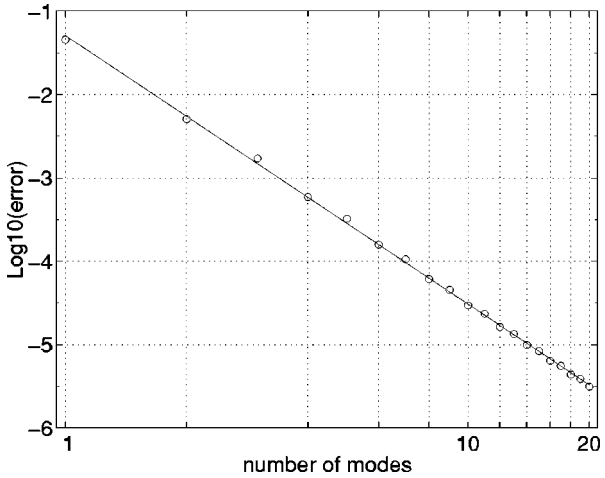

FIG. 4. Convergence of the MMM. The logarithm of the error, $\log(\epsilon)$, is plotted as a function of the number of modes for the same case as Fig. 3.

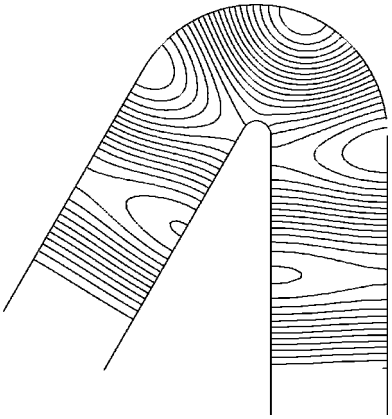

FIG. 5. Contour of the real part of pressure in a duct with $\theta_f = 2.62$ and $h/R_1 = 8$. A plane piston source of frequency such that $kh = 3$ is placed a distance $2h$ upstream from the bend.

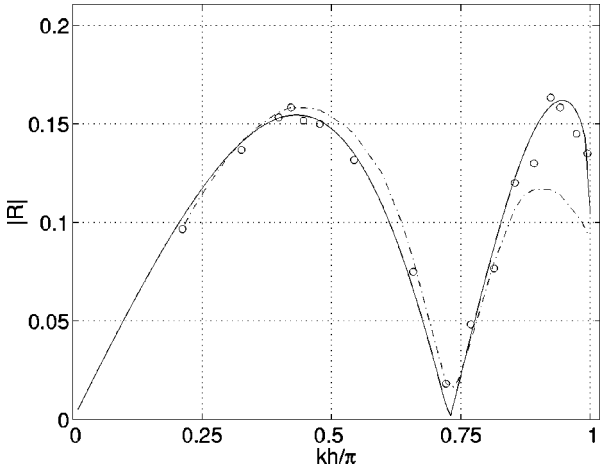

FIG. 6. Variations of the amplitude reflection coefficient with the frequency kh/π. MMM (plain line), finite differences (dashed dotted line, from Cabelli—Ref. 8), experimental results (circles, from Cabelli—Ref. 8) ($\theta_f = 2.62$, $h/R_1 = 8$).

quency parameters, it constitutes an interesting validation of the multimodal method for bends of constant cross section. Moreover the desired solution is a nontrivial solution considering our method, and has been calculated with very good accuracy.

IV. APPLICATION

In this section we show an example of applications of the MMM for the characterization of a particular bend, which has been already characterized by an experiment and a finite differences method calculation in the literature.[8]

The geometry consists in a bend joining two semi-infinite straight ducts, as shown in Fig. 1, with $\theta_f = 2.62$ and $h/R_1 = 8$. The pressure field represented in Fig. 5 with contours of its real part is calculated with 15 modes, using the procedure described in Sec. II C. A condition $P_n = \delta_{n0}$ (piston source) is imposed at a distance $2h$ upstream from the bend, and the frequency of analysis is such that $kh = 3$. This frequency being under the first cutoff frequency, the plane wave is the only propagating mode in the straight sections of the duct system considered here. Thus we can see the distortion of the pressure distribution profiles, and the influence of the evanescent modes in the straight sections, even relatively far from the junction with the bend.

The amplitude reflection coefficient for the plane wave mode (see Pagneux *et al.*[10] for details) is calculated at the inlet of the bend in the duct system previously described and is given in Fig. 6 as a function of the frequency parameter kh, varying between 0 and π. The algebraic method presented in Appendix D gives similar results to our method, as expected. Experimental and numerical results of Cabelli[8] for the same geometry are also reported. The multimodal method gives results in good agreement with the experimental measurements. While the finite difference calculation of Cabelli seems to give satisfying results for low frequency, values near the cutoff are underestimated. As anechoic termination, Cabelli applied a boundary condition a distance $0.8h$ downstream from the bend, ensuring a lack of reflection of the propagative modes and the first nonpropagative mode only. Near the cutoff frequency, this condition may be too limited. Furthermore, the calculation of the standing wave ratio upstream from the bend implies that the wave is plane, without significant evanescent modes, and this hypothesis may cause considerable errors near the cutoff. Such errors are avoided with the multimodal method, since a sufficiently large number of evanescent modes can be taken into account, in order to get accurate results.

V. VARYING CROSS SECTION CURVED DUCTS

In this section, the study initiated by Pagneux *et al.*[10,11] for two-dimensional varying cross section waveguides of straight longitudinal axis is extended to curved ducts with varying cross section, as shown in Fig. 7, where notations are defined. A new Riccati equation is derived and we present results obtained with this generalized formulation.

A. Formulation

The basis functions ψ_n are now functions of both r and θ :

$$\psi_n(r,\theta) = \sqrt{\frac{2-\delta_{n0}}{R_2(\theta)-R_1(\theta)}}\cos\left(n\pi\frac{r-R_1(\theta)}{R_2(\theta)-R_1(\theta)}\right). \tag{32}$$

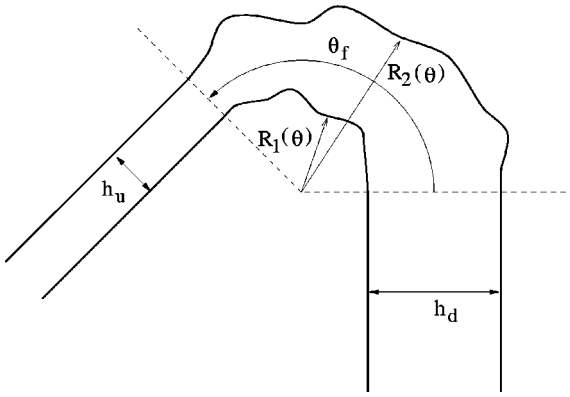

FIG. 7. Geometry of the duct system with varying cross section curved duct and notations.

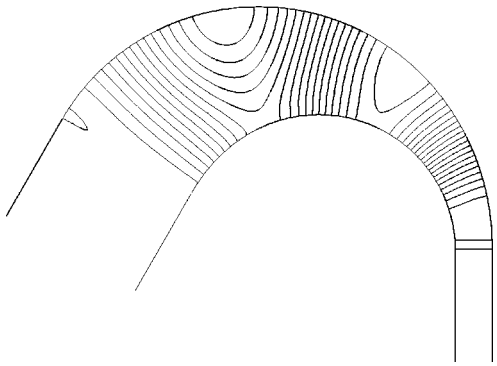

FIG. 8. Contour of the real part of pressure in a trunk with $\theta_f=2.62$, $h_u/h_d=4$ and $R_1(\theta)$ and $R_2(\theta)$ given, respectively, by Eqs. (38) and (39) (see Fig. 7). A plane piston source of frequency such that $kh_e=3$ is placed at the inlet of the curved part.

Furthermore, the boundary condition is now $\partial_n p=0$ on the hard walls. Paying attention to these remarks, we project Eqs. (5) and (6) on the set of functions ψ_n to find (see Appendix E)

$$\mathbf{U}'=\frac{1}{jk}(C+KB)\mathbf{P}-D\mathbf{U}, \tag{33}$$

$$\mathbf{P}'=-jkB\mathbf{U}+(E-D)\mathbf{P}, \tag{34}$$

where

$$D_{mn}=\begin{cases}\dfrac{R_2'-R_1'}{R_2-R_1}\left(1-\dfrac{\delta m0}{2}\right) & \text{for } m=n\\[2ex] A_mA_n((-1)^{m+n}R_2'-R_1')\dfrac{m^2}{m^2-n^2} & \text{for } m\neq n\end{cases} \tag{35}$$

and

$$E_{mn}=A_mA_n((-1)^{m+n}R_2'-R_1'). \tag{36}$$

Equations (33) and (34), combined with Eq. (19), lead to the new Riccati equation:

$$Z'=-jkB-\frac{1}{jk}Z(C+KB)Z+ZD-DZ+EZ. \tag{37}$$

We thus recognize Eqs. (14), (15), and (20) with additional terms. These terms are functions of R_1' and R_2', i.e., the variations of the cross section.

The same numerical procedures as described in Sec. II C can then be used to calculate the acoustic field or the reflection coefficient matrix of such geometries.

B. Results

The duct system considered here is the ''elephant's trunk'' represented in Fig. 8. The widths of the two semi-infinite straight ducts are such that $h_u/h_d=4$ and R_1 and R_2 are given by

$$R_1(\theta)=(h_u-h_d)\left(\frac{\theta}{\theta_f}\right)^3-\frac{3}{2}(h_u-h_d)\left(\frac{\theta}{\theta_f}\right)^2+R_m-\frac{h_d}{2} \tag{38}$$

and

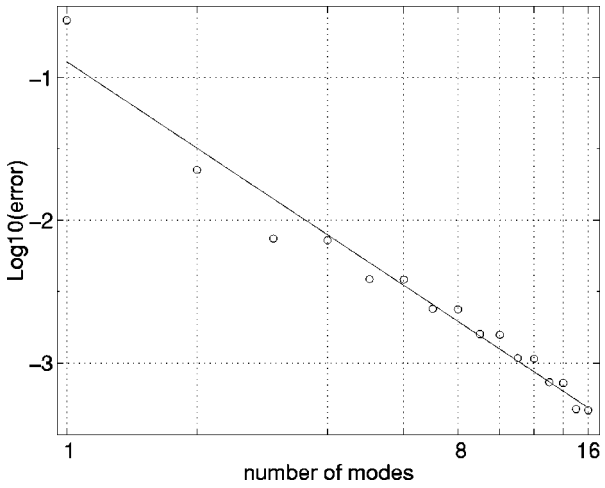

FIG. 9. Convergence of the MMM, in the case of the elephant's trunk (see Fig. 8). The logarithm of the error, $\log(\epsilon)$, is plotted as a function of the number of modes.

$$R_2(\theta)=(h_d-h_u)\left(\frac{\theta}{\theta_f}\right)^3-\frac{3}{2}(h_d-h_u)\left(\frac{\theta}{\theta_f}\right)^2+R_m+\frac{h_d}{2}, \tag{39}$$

where $R_m=1.25h_u$ and $\theta_f=2.62$. The pressure field (real part) shown in Fig. 8 has been calculated using 20 modes, and with a frequency such that $kh_u=3$. A plane piston source is imposed at the inlet of the trunk.

In order to measure the rate of convergence of the reformulated method, the result obtained with 20 modes is chosen as the reference, and we calculate the error (31) as a function of the number of modes taken into account. The error is shown in Fig. 9: The convergence follows a $1/N^{2\pm0.5}$ law, N being the number of modes introduced in the calculation. The convergence rate is lower than in the case of a constant cross section, although it remains high, because the basis functions ψ_n do not satisfy the boundary condition of vanishing normal derivative. Furthermore, one should mention that the convergence rate of an error based on derivatives of the pressure would also decrease. Work is in progress to improve the convergence by taking mixed basis of functions.[17]

Moreover, we can see in Fig. 9 an unexpected behavior: The addition of antisymmetric transverse modes (N even) in the calculation seems to have no effect on the error, as if their contribution to the solution was negligible, with the exception of the first antisymmetric mode. This is probably due to the nature of the coupling between the modes. We recall that two ways of coupling are to be considered in such geometry: One due to the curvature of the duct and the other due to the varying cross section. The first may contribute to generation of the first higher order modes only, the second being then preponderant for the remaining higher order modes. This latter is responsible for generation of symmetric modes only, because of the nature of the source (a plane piston) in our example. It may explain the weak influence of the antisymmetric modes.

Reflection coefficient. For the trunk described previously, the amplitude reflection coefficient is calculated at the

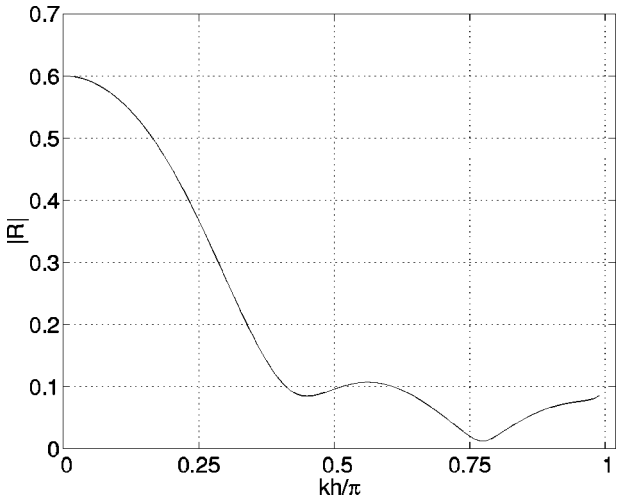

FIG. 10. Variations of the amplitude reflection coefficient with the frequency kh_u/π, calculated at the inlet of a trunk, as described in Fig. 8.

inlet of the curved part ($\theta=\theta_f$) and given in Fig. 10 as a function of the frequency parameter kh_u, varying between 0 and π.

As could be expected, the reflection coefficient tends toward

$$\left|\frac{h_e-h_s}{h_e+h_s}\right|=0.6 \tag{40}$$

for $kh_u=0$. This limit value corresponds to the low frequency reflection coefficient of a section discontinuity in a straight duct. As in the case of a circular bend, the effects of curved ducts vanish at low frequency.

VI. CONCLUSION

A multimodal method for the calculation of the sound propagation in bends has been formulated and validated. It is suitable for any dimension of bend and in any domain of frequency. In contrast to the bend mode method, the difficulties related to the necessary calculation, for each frequency, of the angular wave numbers are avoided. This approach is also convenient both for the formulation of radiation conditions and when considering junctions with ducts of various geometries, such as straight waveguides with varying cross section that have already been treated by modal decomposition.[10,11]

The influence of the evanescent modes generated at the discontinuities on both sides of the bend has been studied, showing the importance of a method that takes into account these evanescent modes.

The multimodal method has been successfully generalized to curved ducts with varying cross section, showing the large field of applications of this method.

Work is in progress to formulate the multimodal method to three-dimensional bends of circular cross section, in which the wave equation is not separable.

APPENDIX A

We want to project the equation of momentum conservation $-jkrv_\theta=\partial p/\partial\theta$ on the basis of functions ψ_n. We have, for any $m\geqslant 0$,

$$-jk\int_{R_1}^{R_1+h} rv_\theta\psi_m\,dr=\int_{R_1}^{R_1+h}\frac{\partial p}{\partial\theta}\psi_m\,dr. \tag{A1}$$

Using the series decomposition (7) and (8) of p and v_θ, Eq. (A1) gives

$$-jk\sum_{n\geqslant 0}\left(\int_{R_1}^{R_1+h} r\psi_m\psi_n\,dr\right)U_n=\frac{\partial}{\partial\theta}P_m, \tag{A2}$$

thus

$$-jkB\mathbf{U}=\mathbf{P}', \tag{A3}$$

with B given by Eq. (17).

The procedure is the same for the equation of mass conservation (5).

APPENDIX B

We give in this appendix the expressions for the matrices B and C defined in Sec. II A [Eqs. (17) and (18)]:

$$B_{mn}=\begin{cases} R_1+\dfrac{h}{2} & \text{for } m=n \\ A_mA_n\left(\dfrac{h}{\pi}\right)^2((-1)^{m+n}-1)\dfrac{m^2+n^2}{(m^2-n^2)^2} & \text{for } m\neq n \end{cases} \tag{B1}$$

$$C_{mn}=\begin{cases} 0 & \text{for } m=n \\ A_mA_n((-1)^{m+n}-1)\dfrac{m^2}{m^2-n^2} & \text{for } m\neq n. \end{cases} \tag{B2}$$

APPENDIX C

Considering the duct system of Fig. 1, Z, $\mathbf{U}$, and $\mathbf{P}$ can be calculated in the straight region upstream from the bend, where P and U satisfy[10]

$$\mathbf{P}^{(S)}=D_1\mathbf{P}^{(I)}+D_2Z_c\mathbf{U}^{(I)} \tag{C1}$$

and

$$\mathbf{U}^{(S)}=D_2Z_c^{-1}\mathbf{P}^{(I)}+D_1\mathbf{U}^{(I)}, \tag{C2}$$

where the superscripts (I) and (S) indicate, respectively, the inlet of the bend and a point upstream, the two being distant from d, as shown in Fig. 1, D_1 and D_2 are diagonal and defined by $D_1=\cos(k_nd)$ and $D_2=j\sin(k_nd)$. Substituting Eq. (19) into Eq. (C1) and defining $D_3=j\tan(k_nd)$, we can obtain a relation between the impedance at the point S upstream from the bend and its value $Z^{(I)}$ at the inlet:

$$Z^{(S)}=D_3(I+D_2^{-1}Z^{(I)}(Z^{(I)}+D_3^{-1}Z_c)^{-1}D_2^{-1})Z_c, \tag{C3}$$

where I is the identity matrix. It is now possible to propagate the pressure or velocity down the straight duct by using

$$\mathbf{U}^{(I)}=(-D_2Z_c^{-1}(Z^{(S)}-Z_c)+e^{-jk_nd})\mathbf{U}^{(S)} \tag{C4}$$

derived from Eqs. (C1) and (C2).

Equation (C4) is greatly simplified in the semi-infinite straight duct downstream from the bend, since the impedance at each point is the characteristic impedance Z_c.

APPENDIX D

An algebraic method for the calculation of the reflection and transmission matrices, in the same manner as Tam,[7] is developed in this appendix.

The duct system studied is represented in Fig. 1, consisting in a bend joining two semi-infinite straight ducts. The incident and reflected waves in region (I) and the transmitted wave in region (III) can be written as follows:

$$p^{(i)}=\sum_n P_n^{(i)}\psi_n(x)e^{j(\omega t-k_n z)}, \tag{D1}$$

$$p^{(r)}=\sum_n P_n^{(r)}\psi_n(x)e^{j(\omega t+k_n z)}, \tag{D2}$$

and

$$p^{(t)}=\sum_n P_n^{(t)}\psi_n(\zeta)e^{j(\omega t-k_n \eta)}. \tag{D3}$$

In region (II), we deduce from Eqs. (14) and (15) a second-order differential equation for $\mathbf{P}$:

$$\mathbf{P}''+B(C+KB)\mathbf{P}=0. \tag{D4}$$

A general solution of Eq. (D4) can be constructed in terms of the eigenvalues $\nu_1^2,\nu_2^2,\ldots$ and eigenvectors $\boldsymbol{\alpha}_1,\boldsymbol{\alpha}_2,\ldots$ of the matrix $B(C+KB)$:

$$\mathbf{P}=XD(\theta)\mathbf{C}_1+XD^{-1}(\theta)\mathbf{C}_2, \tag{D5}$$

where $X=[\boldsymbol{\alpha}_1,\boldsymbol{\alpha}_2,\ldots]$, $D(\theta)$ is diagonal and given by

$$D_n(\theta)=e^{j\nu_n\theta} \tag{D6}$$

with

$$\nu_n=\begin{cases}\sqrt{\nu_n^2} & \text{for propagative modes,}\\ -j\sqrt{-\nu_n^2} & \text{for evanescent modes,}\end{cases} \tag{D7}$$

$\mathbf{C}_1$ and $\mathbf{C}_2$ are arbitrary constant column vectors. The term $XD(\theta)\mathbf{C}_1$ in Eq. (D5) corresponds thus to the right going waves [toward region (III)], while the second term corresponds to the left going waves [toward the region (I)].

We now match the solution for the pressure in the bend and its normal derivative to the external solutions (D1), (D2), and (D3).

At $\theta=0$,

$$\mathbf{P}^{(t)}=X(\mathbf{C}_1+\mathbf{C}_2), \tag{D8}$$

$$jkE\mathbf{P}^{(t)}=B^{-1}X\nu^{-1}(\mathbf{C}_1-\mathbf{C}_2), \tag{D9}$$

and similarly at $\theta=\theta_f$,

$$\mathbf{P}^{(i)}+\mathbf{P}^{(r)}=XD\mathbf{C}_1+XD^{-1}\mathbf{C}_2, \tag{D10}$$

$$jkE(\mathbf{P}^{(i)}-\mathbf{P}^{(r)})=B^{-1}X\nu^{-1}(D\mathbf{C}_1-D^{-1}\mathbf{C}_2), \tag{D11}$$

with $D=D(\theta_f)$, E is diagonal and given by $E_n=k_n/k$, and where the n^{th} term of the diagonal matrix ν is $1/j\nu_n$. We have $B^{-1}X\nu^{-1}=-jkHY$, with $H=(1/jk)(C+KB)$ and $Y=X\nu$. Equations (D8)–(D11) thus become

$$\mathbf{P}^{(t)}=X(\mathbf{C}_1+\mathbf{C}_2), \tag{D12}$$

$$-E\mathbf{P}^{(t)}=HY(\mathbf{C}_1-\mathbf{C}_2), \tag{D13}$$

$$\mathbf{P}^{(i)}+\mathbf{P}^{(r)}=XD\mathbf{C}_1+XD^{-1}\mathbf{C}_2, \tag{D14}$$

$$-E(\mathbf{P}^{(i)}-\mathbf{P}^{(r)})=HY(D\mathbf{C}_1-D^{-1}\mathbf{C}_2). \tag{D15}$$

The reflection matrix R and the transmission matrix T are defined, respectively, by $\mathbf{P}^{(r)}=R\mathbf{P}^{(i)}$ and $\mathbf{P}^{(t)}=T\mathbf{P}^{(i)}$. We find them by solving the set of equations above, taking care to keep only the matrix D^{-1} in the expressions of R and T. D is indeed a source of numerical problems, since terms such as $\exp(\sqrt{-\nu_n^2}\theta_f)$ can be exceedingly large when ν_n^2 is large and negative. We thus find

$$R=-\Delta^{-1}\tilde{\Delta}, \tag{D16}$$

$$T=4\Delta^{-1}D^{-1}(EX-HY)^{-1}E, \tag{D17}$$

with

$$\Delta=D^{-1}(EX-HY)^{-1}(EX+HY)\times D^{-1}(X^{-1}+Y^{-1}H^{-1}E)+(X^{-1}-Y^{-1}H^{-1}E), \tag{D18}$$

$$\tilde{\Delta}=(X^{-1}+Y^{-1}H^{-1}E)+D^{-1}(EX-HY)^{-1}\times(EX+HY)D^{-1}(X^{-1}-Y^{-1}H^{-1}E). \tag{D19}$$

APPENDIX E

We give in this appendix useful elements to project the two Euler equations (5) and (6), paying attention to the dependence of the basis functions ψ_n with θ and to the correct boundary condition

$$\frac{\partial p}{\partial n}=\frac{\partial p}{\partial r}-\frac{R'}{R^2}\frac{\partial p}{\partial \theta}=0. \tag{E1}$$

We use Leibniz's rule to get the projection for $\partial p/\partial\theta$ and $\partial v_\theta/\partial\theta$. From

$$\int_{R_1}^{R_2}\frac{\partial p}{\partial\theta}\psi_m\,dr=\int_{R_1}^{R_2}\frac{\partial(p\psi_m)}{\partial\theta}dr-\int_{R_1}^{R_2}p\frac{\partial\psi_m}{\partial\theta}dr, \tag{E2}$$

we deduce

$$\int_{R_1}^{R_2}\frac{\partial p}{\partial\theta}\psi_m\,dr=\frac{\partial}{\partial\theta}\left(\int_{R_1}^{R_2}p\psi_m\,dr\right)-\int_{R_1}^{R_2}p\frac{\partial\psi_m}{\partial\theta}dr-R_2'[p\psi_m](R_2)+R_1'[p\psi_m](R_1), \tag{E3}$$

which implies

$$\int_{R_1}^{R_2}\frac{\partial p}{\partial\theta}\psi_m\,dr=P_m'+D_{mn}P_n-E_{mn}P_n, \tag{E4}$$

with the matrices D and E given by Eqs. (35) and (36).

Moreover, when projecting $\partial_r(r\partial_r p)$ in Eq. (5), a term $[r(\partial_r p)\psi_m]_{R_1}^{R_2}$ appears. We calculate this term by substituting Eq. (6) into Eq. (E1), to obtain

$$\frac{\partial p}{\partial r}=-jk\frac{R'}{R}u. \tag{E5}$$

Finally, we have

$$\left[r \frac{\partial p}{\partial r} \psi_m \right]_{R_1}^{R_2} = -jkE_{mn}U_{mn}. \tag{E6}$$

[1] W. Rostafinski, ''Monograph on propagation of sound waves in curved ducts,'' NASA Reference Publ. 1248 (1991).
[2] P. E. Krasnushkin, ''On waves in curved tubes,'' Uch. Zap. Mosk. Gos. Univ. **75**, 9–27 (1945).
[3] F. E. Grigor'yan, ''Theory of sound wave propagation in curvilinear waveguides,'' Akust. Zh. **14**, 376–384 (1968) [English translation: Sov. Phys. Acoust. **14**, 315–321 (1969)].
[4] W. Rostafinski, ''On propagation of long waves in curved ducts,'' J. Acoust. Soc. Am. **52**, 1411–1420 (1972).
[5] A. Cummings, ''Sound transmission in curved duct bends,'' J. Sound Vib. **35**, 451–477 (1974).
[6] W. C. Osborne, ''Higher mode propagation of sound in short curved bends of rectangular cross section,'' J. Sound Vib. **45**, 39–52 (1976).
[7] C. K. W. Tam, ''A study of sound transmission in curved duct bends by the Galerkin method,'' J. Sound Vib. **45**, 91–104 (1976).
[8] A. Cabelli, ''The acoustic characteristics of duct bends,'' J. Sound Vib. **68**, 369–388 (1980).
[9] R. P. Dougherty, ''A Wave-splitting technique for nacelle acoustic propagation,'' AIAA Pap. **97**, 1652 (1997).
[10] V. Pagneux, N. Amir, and J. Kergomard, ''A study of wave propagation in varying cross section waveguides by modal decomposition. Part I. Theory and validation,'' J. Acoust. Soc. Am. **100**, 2034–2048 (1996).
[11] N. Amir, V. Pagneux, and J. Kergomard, ''A study of wave propagation in varying cross section waveguides by modal decomposition. Part II. Results,'' J. Acoust. Soc. Am. **101**, 2504–2517 (1997).
[12] A. F. Stevenson, ''Exact and approximate equations for wave propagation in acoustic horns,'' J. Appl. Phys. **22**, 1461–1463 (1951).
[13] R. J. Albertson, ''The propagation of sound in a circular duct of continuously varying cross-sectional area,'' J. Sound Vib. **23**, 433–442 (1972).
[14] A. Roure, ''Propagation guidée, étude des discontinuités,'' Doctoral thesis, Université d'Aix-Marseille, 1976.
[15] J. Kergomard, ''Calculation of discontinuities in waveguides using mode-matching method: An alternative to the scattering matrix approach,'' J. Acoust. **4**, 111–137 (1991).
[16] K. Lin and R. L. Jaffe, ''Bound state and threshold resonances in quantum wires with circular bends,'' Phys. Rev. B **54**, 5750–5762 (1996).
[17] C. Hazard and V. Pagneux, ''Improved multimodal approach in waveguides with varying cross-section,'' accepted in 17th I.C.A., Rome (2001).